

A NUMERICAL STUDY ON THE EFFECT OF MAGNETIC HEATING TO CRUDE OIL-NANOFLUID FLOW FOR ENHANCED OIL RECOVERY

P. H. Tan^a, K. S. Fong^a, A. Y. Mohd Yassin^{b*}, M. Latheef^a

^aDepartment of Civil and Environmental Engineering, Universiti Teknologi PETRONAS, Perak, Malaysia

^bSchool of Energy, Geoscience, Infrastructure and Society, Heriot-Watt University, Putrajaya, Malaysia

Article history

Received

8 August 2019

Received in revised form

25 November 2019

Accepted

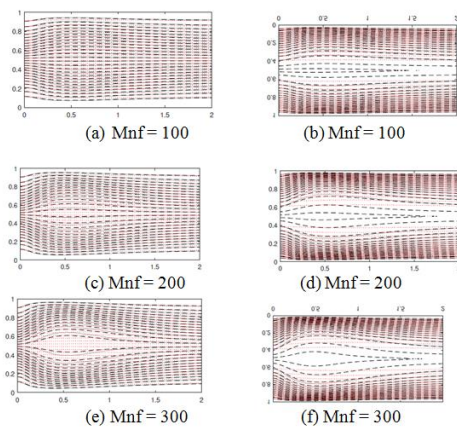
16 January 2020

Published online

27 February 2020

*Corresponding author
a.mohd_yassin@hw.ac.uk

Graphical abstract



Abstract

Magnetic heating of crude oil mixed with nanoparticle for heat transfer mechanism enhancement has received much attention in enhanced oil recovery (EOR). In the present work, the heat transfer of Fe_3O_4 , Al_2O_3 , CuO , Cu nanoparticles mixed in crude oil is theoretically investigated. The mathematical model of magnetic field heating in reservoir is represented by the channel flow of crude oil-nanofluid subjected to a longitudinal spatially varying magnetic field. The viscous incompressible flow is bounded by nonisothermal walls. The coupled nonlinear partial differential equations (PDEs) are solved numerically using an unconditionally stable time integration and finite element method. The numerical results are validated against data available in literature. The physical aspects of the crude oil-nanofluid flow and heat transfer are discussed in terms of several pertinent parameters such as solid nano fraction, skin friction, magnetic, Hartmann and Nusselt numbers. It is found that the enhancement of heat transfer increases with the magnetic number and solid nano fraction while decreases with the increase in Hartmann number. It is shown that, the addition of nanoparticle and increment of magnetic number is effective in the localised heating. In addition, the heat transfer of Fe_3O_4 , Al_2O_3 , CuO , Cu nanoparticles in crude oil mixed are investigated and assessed against each other. It is observed that, the heating mechanism would not be as effective for high electrically conducting nanoparticles. The results also indicate that nanoparticle with high thermal conductivity and low electrical conductivity is preferable in obtaining susceptible thermal heating for the EOR.

Keywords: Nanoparticles, nanofluids, crude oil, finite element method, magnetic heating, EOR

Abstrak

Pemanasan magnetik minyak mentah yang dicampur dengan zarah nano untuk tujuan peningkatan mekanisma pemindahan haba telah mendapat perhatian para penyelidik dalam bidang perolehan minyak tertingkat (EOR). Dalam kajian ini, pemindahan haba zarah nano Fe_3O_4 , Al_2O_3 , CuO , dan Cu dalam campuran minyak mentah dikaji secara teori. Model matematik pemanasan magnetik di dalam takungan diwakili oleh aliran saluran yang ditindaki oleh medan magnetik yang berubah secara membujur. Aliran likat tidak termampat telah disempadani dinding penyepuhlindungan sesuhu. Persamaan pembezaan separa (PDEs) terganggu tak linear diselesaikan secara berangka menggunakan kaedah unsur terhingga dengan pengamiran masa yang stabil tanpa syarat. Keputusan berangka disahkan

melalui perbandingan data sedia ada. Fizikal aliran minyak mentah dicampuri zarah nano dan pemindahan haba yang berkaitan dibincangkan dari aspek beberapa parameter penting seperti pecahan pepejal-nano, geseran kulit, nombor magnetik, nombor Hartmann dan nombor Nusselt. Hasil kajian telah menunjukkan peningkatan pemindahan haba dengan penambahan nombor magnetik dan pecahan pepejal-nano dan menurun dengan penambahan nombor Hartmann. Campuran zarah nano dan penambahan nombor magnetik telah meningkatkan keberkesanan pemanasan setempat. Kadar pemindahan haba nano partikel Fe_3O_4 , Al_2O_3 , CuO , dan Cu telah dibandingkan dan dinilai antara satu sama lain. Pemerhatian telah mendapati bahawa mekanisma pemanasan tidak begitu berkesan untuk zarah nano yang mempunyai keberaliran elektrik yang tinggi. Hasil kajian juga telah menunjukkan zarah nano yang mempunyai keberaliran haba yang tinggi dan keberaliran elektrik yang rendah adalah bersesuaian dalam menghasilkan pemanasan terma untuk tujuan EOR.

Kata kunci: Zarah nano, cecair nano, minyak mentah, kaedah unsur terhingga, pemanasan magnetik, EOR

© 2020 Penerbit UTM Press. All rights reserved

1.0 INTRODUCTION

Crude oil recovery refers to the extraction of residual oil that cannot be accessed using conventional techniques. In general, there are two levels of recovery; secondary and tertiary, respectively. The secondary recovery employs solvent injection to drive the residual oil into the collection well for extraction purposes. Although the recovery rate might go up to 20 per cent [1], heavy crude oil, i.e. oil with a high viscosity cannot be easily swept through by solvent injection. The abundance of heavy crude oil in some oil fields has motivated the tertiary recovery which is synonymously recognised as the enhanced oil recovery (EOR). The common strategy in promoting oil mobility is to decrease the oil viscosity [2]. In this regard, popular methods such as steam assisted gravity drainage (SAGD) [3, 4] and electromagnetic (EM) heating [5, 6] have been shown to be able to decrease the oil viscosity using thermal effects. It is well known that the viscosity of oil decreases when the temperature increases [7].

Recently, the EM heating method has received much attention because of its remote supply capability where additional heat energy can be achieved at a considerably low level of heat loss [8]. In contrast, the SAGD method requires extensive steam and water supply thus remain less favourable [9]. In the EM heating process, heat is emanated from an electromagnetic source to agitate the oil molecules, thereby increasing the oil temperature and decreasing the oil viscosity. However, the performance of the EM heating method is often limited by the natural characteristics of crude oil, i.e. low thermal conductivity and electrical conductivity. To overcome these, metal nanoparticles can be added, leading to a mixture known as crude oil-nanofluid. It was shown experimentally that the EM heating method can be more effective in increasing the oil temperature with the addition of nanofluid [10,

11]. Therefore, the findings suggest that the combination of EM heating method and nanofluid is a viable improvement to the EOR technology.

Previous studies on the EM heating method [12, 13] and magnetic heating method [14] to crude oil-nanofluid were largely experimental. Providing the theoretical aspects of the latter is the interest of this paper. In the experimental studies, the focus was on the technical feasibility and effectiveness of the aforementioned combination. Physical quantities including recovery rate, viscosity and temperature were investigated from the different experimental settings. The corresponding working mechanism was explained in the context of physical chemistry thus cannot systematically explain the macroscopic flow behaviour of the crude oil-nanofluid. It is of the opinion that, for an optimised recovery, the mechanics of fluid flow and heat transfer ensuing from the interaction between crude oil-nanofluid and magnetic field must be properly investigated. In this regard, a numerical approach based on multiphysics modelling, i.e. coupling between fluid mechanics and electromagnetics is necessary to investigate the interaction between crude oil-nanofluid and magnetic field. Therefore, this study aims to investigate the crude oil-nanofluid flow and heat transfer under the exposure of magnetic field using a numerical approach.

The simpler numerical models related to crude oil modelling (without nanofluid) involved coupling between heat transfer and electromagnetism [15, 16, 17]. The volumetric heat source was described as thermal energy emitted from the EM waves in the longitudinal direction. The heat transfer from EM source to the medium was modelled by the energy balance by considering conduction and convection. Furthermore, the medium of reservoir was treated as isotropic and homogeneous. Their finding showed that, the temperature was increased at the proximity of the source of heating. However, the crude oil

motion was not allowed because only mass and energy balance were employed while conservation of momentum was neglected. Also, in these studies no nanoparticle were added.

While the study on the mathematical modelling of the effect of EM on crude oil (without nanofluid) is sparse, models for general nanofluid are well-established. Various numerical models that account for the conservation of mass, momentum and energy have been proposed for a variety of nanoparticles and based fluids [18, 19, 20, 21]. In these works, nanofluid flow and heat transfer have been investigated for natural convection [18, 19], forced convection [20] and mixed convection [21] under the applied magnetic field.

For works on natural convection [18, 19], the magnetohydrodynamic (MHD) natural convection and heat transfer of nanofluids under the exposure of constant magnetic field were numerically investigated. A square domain bounded by isothermal and linearly heated side walls was selected. Nondimensional numbers namely Hartmann, Rayleigh and Grashof were the governing parameters. It has been shown that, the interaction between electric conducting nanofluid and magnetic field resulted in the rise of Lorentz force which can be represented by Hartman number. The increment in Hartmann number suppressed the heat transfer flow. In addition, the effect of brownian motion of nano particle can be obtained in [22] which is not being considered in current work.

Works on the forced convection in [20] involved a fully developed flow. The spatially varying magnetic field was imposed in the transverse direction to the channel. Both viscous dissipation and Joule heating were considered. Reynolds number was the governing parameter. Magnetisation force and Lorentz force were employed as the forcing terms. The magnetisation force arose due to the addition of nanoparticles and a function of magnetic intensity. The presence of magnetisation force is analogous to the ferrohydrodynamic (FHD) principle [23].

Due to the complexity of the governing equations, numerical methods including finite difference method (FDM) [18, 19, 21], finite volume method (FVM) [20], and finite element method (FEM) [20] were employed. Each numerical method has its advantages and disadvantages, but the common aim is to discretise the problem into algebraic equations and solve using suitable algorithms. Using regular grids, FDM has the strength of being relatively simple to implement. However, FDM is not suitable for complex geometries. Furthermore, FDM is known to exhibit oscillation which may require relaxation scheme to stabilise the solution [24]. FVM is ideal for computational fluid dynamics since the discretised system is solved in conservation form. Furthermore, Neumann boundaries can be naturally imposed in the formulation. However, higher order approximation functions are not usually used. Likewise, FVM is not suitable for unstructured mesh [25]. The aforementioned issues can be resolved using FEM. FEM has been known to display a high degree of

accuracy and stability in nanofluid flow and heat transfer problem [20].

EM and magnetic heating differ in terms of the time-dependent nature of the former. While a theoretical formulation involving EM would be a general one but the mathematical aspects will be very complex. For a pioneering work, a formulation involving time-independent magnetic heating would be the sufficient first step. Thus, it is our interest to study crude oil-nanofluid flow and heat transfer mechanism in EOR using magnetic heating. In this present study, the governing equations of the crude oil-nanofluid flow subjected to parallel varying external magnetic field are solved numerically using the FEM. The effect of pertinent parameters such as the Nusselt number, skin friction, magnetic number, Hartman number and solid nano fraction are then discussed. The mathematical formulation is presented in section 2. In section 3, the numerical results are presented and discussed revolving around the effects of the the pertinent parameters and followed by the discussion on the the the feasibility of magnetic heating for EOR.

2.0 METHODOLOGY

2.1 Governing Equations

Figure 1 shows a schematic representation of two-dimensional channel of length, L and height, h filled with a crude oil-nanofluid. The flow is bounded by top and bottom nonisothermal walls, as well as parabolic inlet and fully developed outflow. The flow is subjected to a spatially varying magnetic field. The oil phase and spherical iron oxide are considered to be in thermal and velocity equilibrium. The radiation effect and displacement current are neglected.

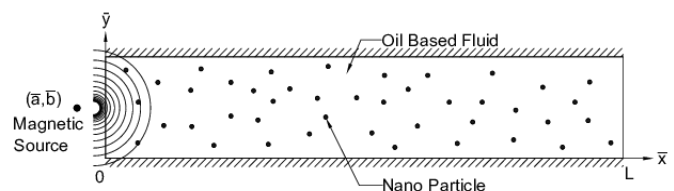


Figure 1 Crude oil mixed with nanoparticles in channel

The fluid motion which includes the magnetic body force for single-phase nanofluid is considered as Newtonian, incompressible and electrically conducting flow. The governing equations can be given in dimensional form as

Continuity equation:

$$\frac{\partial \bar{u}}{\partial \bar{x}} + \frac{\partial \bar{v}}{\partial \bar{y}} = 0 \quad (1)$$

Momentum equation:

$$\rho_{nf} \left(\frac{\partial \bar{u}}{\partial \bar{t}} + \bar{u} \frac{\partial \bar{u}}{\partial \bar{x}} + \bar{v} \frac{\partial \bar{u}}{\partial \bar{y}} \right) = -\frac{\partial \bar{p}}{\partial \bar{x}} + \bar{\mu}_o \bar{M} \frac{\partial \bar{H}}{\partial \bar{x}} + \mu_{nf} \nabla^2 \bar{u} \quad (2)$$

$$\rho_{nf} \left(\frac{\partial \bar{v}}{\partial \bar{t}} + \bar{u} \frac{\partial \bar{v}}{\partial \bar{x}} + \bar{v} \frac{\partial \bar{v}}{\partial \bar{y}} \right) = -\frac{\partial \bar{p}}{\partial \bar{y}} + \bar{\mu}_o \bar{M} \frac{\partial \bar{H}}{\partial \bar{y}} + \mu_{nf} \nabla^2 \bar{v} - \sigma_{nf} \bar{B}^2 \bar{v} \quad (3)$$

Energy equations:

$$(\rho c_p)_{nf} \left(\frac{\partial \bar{T}}{\partial \bar{t}} + \bar{u} \frac{\partial \bar{T}}{\partial \bar{x}} + \bar{v} \frac{\partial \bar{T}}{\partial \bar{y}} \right) + \bar{\mu}_o \bar{T} \frac{\partial \bar{M}}{\partial \bar{T}} \left(\bar{u} \frac{\partial \bar{H}}{\partial \bar{x}} + \bar{v} \frac{\partial \bar{H}}{\partial \bar{y}} \right) - \sigma_{nf} \bar{B}^2 \bar{v}^2 = k_{nf} \nabla^2 \bar{T} + \mu_{nf} \left[2 \left(\frac{\partial \bar{u}}{\partial \bar{x}} \right)^2 + 2 \left(\frac{\partial \bar{v}}{\partial \bar{y}} \right)^2 + \left(\frac{\partial \bar{v}}{\partial \bar{x}} + \frac{\partial \bar{u}}{\partial \bar{y}} \right)^2 \right] \quad (4)$$

Maxwell equation and Ohm's Law:

$$\begin{aligned} \nabla \times \mathbf{H} &= \mathbf{J} = \sigma(\mathbf{v} \times \mathbf{B}) \\ \nabla \cdot \mathbf{B} &= \nabla \cdot (\mathbf{H} + \mathbf{M}) \end{aligned} \quad (5)$$

where \bar{u} and \bar{v} are the velocity component in \bar{x} and \bar{y} direction, \bar{p} is the pressure and \bar{T} is the local temperature of the nanofluid, \bar{t} is time, ρ is the density, k is the thermal conductivity, c_p is the specific heat capacity, α is the thermal diffusivity, σ is the electrical conductivity, subscript nf refers to nanofluid, μ_o is the viscosity, \bar{H} the magnetic intensity, \bar{M} the magnetisation and \bar{B} is the uniform electromagnetic induction.

The magnetic source is hypothesized as being produced by a magnetic wire installed vertically to the \bar{x} - \bar{y} plane at the location (\bar{a}, \bar{b}) shown. The distribution of magnetic intensity is shown in Figure 2 where the magnetic component in \bar{x} direction, \bar{H}_x , in \bar{y} direction, \bar{H}_y , and the \bar{H} intensity are given as

$$\bar{H}_x = \frac{\bar{y}}{2\pi} \frac{\bar{x} - \bar{a}}{\sqrt{(\bar{x} - \bar{a})^2 + (\bar{y} - \bar{b})^2}} \quad (6)$$

$$\bar{H}_y = \frac{\bar{y}}{2\pi} \frac{\bar{y} - \bar{b}}{\sqrt{(\bar{x} - \bar{a})^2 + (\bar{y} - \bar{b})^2}} \quad (7)$$

$$\bar{H} = \sqrt{\bar{H}_x^2 + \bar{H}_y^2} \quad (8)$$

where \bar{y} is the magnetic strength at the point $(\bar{x} = \bar{a}, \bar{y} = \bar{b})$. In this study, the magnetic source is located at $(\bar{a} = -0.05, \bar{b} = h/2)$ and led to $\bar{H}_o = \bar{H}(0.5, 0) = \frac{\bar{y}}{2\pi|\bar{a}|}$.

The variation of magnetisation of fluids was obtained experimentally, given as [26]

$$\bar{M} = \bar{K} \bar{H} (T_c - \bar{T}) \quad (9)$$

where \bar{K} is a pyromagnetic coefficient constant while T_c is the curie temperature of the material.

The following equations are the classical nanofluid model used in determining the effective density and heat capacitance [27].

$$\rho_{nf} = (1 - \phi)\rho_f + \phi\rho_p \quad (10)$$

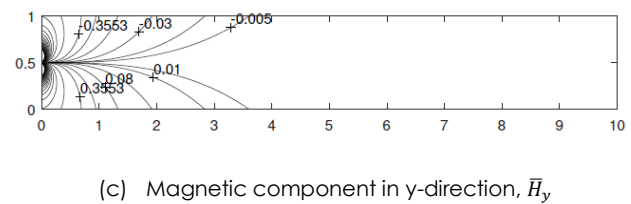
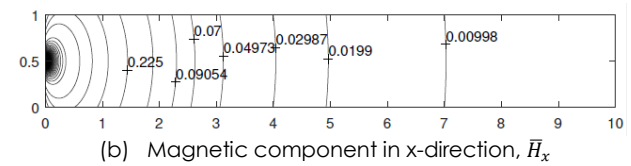
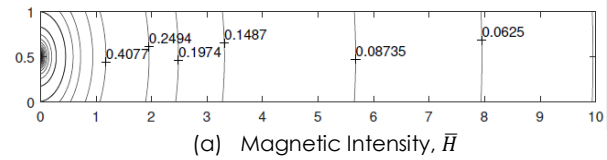


Figure 2 The magnetic distribution of magnetic intensity \bar{H} , \bar{H}_x , and \bar{H}_y

where ϕ is the solid volume fraction, f and p denote based fluid and nanoparticle, respectively.

$$(\rho c_p)_{nf} = (1 - \phi)(\rho c_p)_f + \phi(\rho c_p)_p \quad (11)$$

The effective dynamic viscosity of a spherical particle is approximated using Brinkman model [28]

$$\mu_{nf} = \mu_f (1 - \phi)^{-2.5} \quad (12)$$

and Maxwell-Garnett model is used to express the thermal conductivity of the nanofluid

$$\frac{k_{nf}}{k_f} = \frac{k_p + 2k_f - 2\phi(k_f - k_p)}{k_f + 2k_f - 2\phi(k_f - k_p)} \quad (13)$$

The effective electrical conductivity of the nanofluid [29] can be defined as

$$\frac{\sigma_{nf}}{\sigma_f} = 1 + \frac{3 \left(\frac{\sigma_p - 1}{\sigma_f} \right) \phi}{\left(\frac{\sigma_p + 2}{\sigma_f} \right) - \left(\frac{\sigma_p - 1}{\sigma_f} \right) \phi} \quad (14)$$

By introducing the following non-dimensional variables

$$\begin{aligned}
 x &= \frac{\bar{x}}{h}, & y &= \frac{\bar{y}}{h} \\
 u &= \frac{\bar{u}}{u_r}, & v &= \frac{\bar{v}}{u_r} \\
 T &= \frac{T_w - \bar{T}}{\bar{T}_w - \bar{T}_f}, & H &= \frac{\bar{H}}{H_o} \\
 p &= \frac{\bar{p}}{\rho_{nf} u_r^2}, & t &= \frac{u_r \bar{t}}{h}
 \end{aligned} \quad (15)$$

Equations (1) - (4) are converted into dimensionless form as

Continuity equation:

$$\frac{\partial u}{\partial x} + \frac{\partial v}{\partial y} = 0 \quad (16)$$

Momentum equation:

$$\begin{aligned}
 \frac{\partial u}{\partial t} + u \frac{\partial u}{\partial x} + v \frac{\partial u}{\partial y} + \frac{\partial p}{\partial x} + \frac{1}{Re} \left(\frac{\mu_{nf} \rho_f}{\mu_f \rho_{nf}} \right) \nabla^2 u - \\
 Mn_F \left(\frac{\rho_f}{\rho_{nf}} \right) H \frac{\partial H}{\partial x} T = 0
 \end{aligned} \quad (17)$$

$$\begin{aligned}
 \frac{\partial v}{\partial t} + u \frac{\partial v}{\partial x} + v \frac{\partial v}{\partial y} + \frac{\partial p}{\partial y} + \frac{1}{Re} \left(\frac{\mu_{nf} \rho_f}{\mu_f \rho_{nf}} \right) \nabla^2 v - \\
 Mn_F \left(\frac{\rho_f}{\rho_{nf}} \right) H \frac{\partial H}{\partial y} T + \frac{Ha^2}{Re} H^2 v = 0
 \end{aligned} \quad (18)$$

Energy equation:

$$\begin{aligned}
 \frac{\partial T}{\partial t} + u \frac{\partial T}{\partial x} + v \frac{\partial T}{\partial y} + Mn_F Ec \left(\frac{\rho C_p}{\rho C_p}_{nf} \right) H \left(u \frac{\partial H}{\partial x} + \right. \\
 \left. v \frac{\partial H}{\partial y} \right) (\varepsilon - T) - \frac{1}{Re Pr} \left(\frac{k_{nf} (\rho C_p)_{nf}}{k_f (\rho C_p)_{nf}} \right) \nabla^2 T + \frac{Ha^2}{Re} Ec H^2 v^2 - \\
 \frac{Ec}{Re} \left(\frac{\mu_{nf} (\rho C_p)_{nf}}{\mu_f (\rho C_p)_{nf}} \right) \left(2 \left(\frac{\partial u}{\partial x} \right)^2 + 2 \left(\frac{\partial v}{\partial y} \right)^2 + \left(\frac{\partial v}{\partial x} + \frac{\partial u}{\partial y} \right)^2 \right) = 0
 \end{aligned} \quad (19)$$

which then forming the following non-dimensional parameters

$$\begin{aligned}
 Re &= \frac{\rho_f h u_r}{\mu_f}, & Pr &= \frac{\mu_f C_p}{k_f} \\
 Ec &= \frac{\rho_f u_r^2}{(\rho C_p)_{nf} \Delta T}, & Mn_F &= \frac{\mu_o \bar{H}_o^2 \bar{K} T}{\rho_f u_r^2} \\
 \varepsilon &= \frac{\bar{T}_w}{\bar{T}_w - \bar{T}_f}, & Ha &= h \bar{H}_o \mu_o \sqrt{\frac{\sigma_f}{\mu_f}}
 \end{aligned} \quad (20)$$

These are Reynolds number, Prandtl number, Eckert number and magnetic number, temperature number, and Hartmann number, respectively.

2.2 Boundary Conditions

The inlet flow is assumed to be fully developed with a parabolic profile. Normal derivative of flow field variables (u, v, T) and pressure condition is set to be zero at the outlet. Both the bottom and top walls are thermally insulated and non-slip boundary conditions are imposed for the velocities. Thus, the relevant boundary conditions for the governing equations are as follows

$$\begin{aligned}
 \text{Initial: } t &= 0, u = v = p = T = 0 \\
 \text{Inlet: } x &= 0, 0 \leq y \leq 1: v = 0, u = T = 4y(y - 1) \\
 \text{Outlet: } x &= 10, 0 \leq y \leq 1: \frac{\partial u}{\partial x} = \frac{\partial v}{\partial x} = \frac{\partial T}{\partial x} = 0 \\
 x &= 10, y = 1: p = 0 \\
 \text{Upperwall: } y &= 1, 0 \leq x \leq 10: u = v = T = 0 \\
 \text{Lowerwall: } y &= 0, 0 \leq x \leq 10: u = v = T = 0
 \end{aligned} \quad (21)$$

2.3 Nusselt Number and Skin Friction

The dimensionless quantities of interest are the local and average values of Nusselt number and skin friction. The local Nusselt Nu and average Nusselt Nu_{avg} along the walls are defined as

$$\begin{aligned}
 Nu &= \frac{k_{nf} \partial T}{k_f \partial y} \Big|_{y=0,1} \\
 Nu_{avg} &= \frac{1}{L} \int_0^L Nu \, dx
 \end{aligned} \quad (22)$$

The local C_f and average $C_{f,avg}$ skin friction are evaluated along the top and bottom wall given as

$$\begin{aligned}
 C_f &= \frac{2\mu_{nf} \partial u}{\rho_{nf} u_r^2 \partial y} \Big|_{y=0,1} \\
 C_{f,avg} &= \frac{1}{L} \int_0^L C_f \, dx
 \end{aligned} \quad (23)$$

2.4 FEM Formulation and Validation

The numerical study adopts finite element discretisation in space and an unconditionally stable finite difference in time. The weak form of the PDEs is developed by integrating the product of equation (16)-(19) and weight functions over the domain. Bubnov Galerkin method is used where the interpolation function is the same as the weighting function. The mixed interpolation function is employed for the pressure-velocity pair to satisfy the Ladyzenskaja-Babuska-Brezzi (LBB) condition. Quadratic shape functions are employed to interpolate the velocities and temperature while linear shape functions are used for the pressure. The assembled equation of system can be written in compact PDEs matrix-vector form as

$$\mathbf{M}\dot{\mathbf{U}} + \mathbf{K}(\mathbf{U})\mathbf{U} = \mathbf{F} \quad (24)$$

where \mathbf{M} is the mass matrix, $\dot{\mathbf{U}}$ is the time derivative vector, $\mathbf{K}(\mathbf{U})$ is the non-linear matrix, \mathbf{F} is the force vector, and \mathbf{U} is the field variable vector that consists

of velocities, temperature and pressure which in expanded form can given as

$$\begin{bmatrix} [M] & 0 & 0 & 0 \\ 0 & [M] & 0 & 0 \\ 0 & 0 & 0 & 0 \\ 0 & 0 & 0 & [M] \end{bmatrix} \begin{pmatrix} \dot{u} \\ \dot{v} \\ \dot{p} \\ \dot{T} \end{pmatrix} + \begin{bmatrix} [K + K_n] & 0 & [K_{px}] & [K_{fx}] \\ 0 & [K + K_n + K_m] & [K_{py}] & [K_{fy}] \\ [K_{pv}] & 0 & 0 & 0 \\ [K_{Tv}] & 0 & [K_T + K_n + K_{Tm}] & 0 \end{bmatrix} \begin{pmatrix} u \\ v \\ p \\ T \end{pmatrix} = - \begin{pmatrix} F_1 \\ F_2 \\ F_3 \\ F_4 \end{pmatrix} \quad (25)$$

where

$$\begin{aligned} [K] &= \frac{1}{Re} \left[\frac{\mu_{nf} \rho_f}{\mu_f \rho_{nf}} \right] \int_{\Omega} \left(\frac{\partial N_i}{\partial x} \frac{\partial N_j}{\partial x} + \frac{\partial N_i}{\partial y} \frac{\partial N_j}{\partial y} \right) d\Omega \\ [K_n] &= \int_{\Omega} N_i \left(u \frac{\partial N_j}{\partial x} + v \frac{\partial N_j}{\partial y} \right) d\Omega \\ [K_m] &= \frac{Mnm}{Re} \left(\frac{\sigma_{nf} \rho_f}{\sigma_f \rho_{nf}} \right) \int_{\Omega} H^2 N_i N_j d\Omega \\ [K_{px}] &= \int_{\Omega} N_i \frac{\partial L_j}{\partial x} d\Omega \\ [K_{py}] &= \int_{\Omega} N_i \frac{\partial L_j}{\partial y} d\Omega \\ [K_{fx}] &= Mn_F \left(\frac{\rho_f}{\rho_{nf}} \right) \int_{\Omega} H \frac{\partial H}{\partial x} N_i N_j d\Omega \\ [K_{fy}] &= Mn_F \left(\frac{\rho_f}{\rho_{nf}} \right) \int_{\Omega} H \frac{\partial H}{\partial y} N_i N_j d\Omega \\ [K_{Tu}] &= -Mn_F Ec \varepsilon \left(\frac{(\rho Cp)_f}{(\rho Cp)_{nf}} \right) \int_{\Omega} H \frac{\partial H}{\partial x} N_i N_j d\Omega - \\ &\quad \frac{Ec}{Re} \left(\frac{\mu_{nf} (\rho Cp)_f}{\mu_f (\rho Cp)_{nf}} \right) \left(2 \int_{\Omega} N_i \frac{\partial u}{\partial x} \frac{\partial N_j}{\partial x} d\Omega + \int_{\Omega} N_i \frac{\partial u}{\partial y} \frac{\partial N_j}{\partial y} d\Omega + \int_{\Omega} N_i \frac{\partial v}{\partial x} \frac{\partial N_j}{\partial x} d\Omega \right) \\ [K_{Tv}] &= -Mn_F Ec \varepsilon \left(\frac{(\rho Cp)_f}{(\rho Cp)_{nf}} \right) \int_{\Omega} H \frac{\partial H}{\partial y} N_i N_j d\Omega - \\ &\quad \frac{Ec}{Re} \left(\frac{\mu_{nf} (\rho Cp)_f}{\mu_f (\rho Cp)_{nf}} \right) \left(2 \int_{\Omega} N_i \frac{\partial v}{\partial y} \frac{\partial N_j}{\partial y} d\Omega + \int_{\Omega} N_i \frac{\partial v}{\partial x} \frac{\partial N_j}{\partial x} d\Omega + \int_{\Omega} N_i \frac{\partial u}{\partial y} \frac{\partial N_j}{\partial x} d\Omega \right) - \\ &\quad \frac{Mn_m}{Re} Ec \int_{\Omega} H^2 N_i N_j v d\Omega \\ [K_T] &= \frac{1}{Re Pr} \left(\frac{k_{nf} (\rho Cp)_f}{k_f (\rho Cp)_{nf}} \right) \int_{\Omega} \left(\frac{\partial N_i}{\partial x} \frac{\partial N_j}{\partial x} + \frac{\partial N_i}{\partial y} \frac{\partial N_j}{\partial y} \right) d\Omega \\ [K_{Tm}] &= -Mn_F Ec \left(\frac{(\rho Cp)_f}{(\rho Cp)_{nf}} \right) \left(\int_{\Omega} N_i u H \frac{\partial H}{\partial x} N_j d\Omega + \int_{\Omega} N_i v H \frac{\partial H}{\partial y} N_j d\Omega \right) \\ [M] &= \int_{\Omega} N_i N_j d\Omega \end{aligned}$$

2.5 Nonlinear Solver

The nonlinear system is solved by using Newton-Raphson scheme. Equation (24) is expressed in the search for fixed point residual after temporal discretisation such that

$$R(U) = \left(\frac{[M]}{\Delta t} + K(U) \right) U^{n+1} - \{F\} - \frac{[M]}{\Delta t} U^n = 0 \quad (26)$$

The truncated Taylor series expansion of $R(U)$ about the known n^{th} solutions can be given as

$$0 = R(U^n) + \frac{\partial R(U)}{\partial U} \Delta U + O(U^2) \quad (27)$$

where $\Delta U = U^{n+1} - U^n$. Omitting higher order term $O(U^2)$ results in

$$R(U^n) = -\frac{\partial R(U)}{\partial U} \Delta U \cong -T(U^n) \Delta U \quad (28)$$

where $T(U^n)$ is the tangent stiffness expressed as

$$T = \frac{[M]}{\Delta t} + \frac{[K(U)]\{U\}^{n+1}}{\partial \{U\}^{n+1}} \quad (29)$$

The problem is simultaneously solved by the change of field quantities

$$\Delta U = -[T^{-1}(U^n)]R(U^n) \quad (30)$$

The updated solution is given as

$$U^{n+1} = U^n + \Delta U \quad (31)$$

The final solution is obtained when convergence tolerance of the norm residual is less than 10^{-5} for all field variables. The complete numerical scheme was implemented in MATLAB. Unstructured triangular mesh system is generated with the grid being finer in the proximity of the magnetic source while coarser at the downstream. Several mesh were tested for mesh independent solution as shown in Figure 3. It was observed that 24112 of elements ensures mesh independent solution. The flowchart of the nonlinear scheme is shown in Figure 4 which the step-by-step description is given below.

- STEP 1: take or assume a known value of $\{U\}^{n-1}$
- STEP 2: use the known $\{U\}^{n-1}$ to calculate the global tangent stiffness matrix, $[T]^{n-1}$
- STEP 3: calculate the residual, $\{R\}$
- STEP 4: solve the vector of incremental dof, $\{\Delta U\}$
- STEP 5: update $\{U\}^n$ and check for convergence
- STEP 6: if converge, stop iteration else repeat STEP 2 by using the just updated $\{U\}^r$ as $\{U\}^{n-1}$

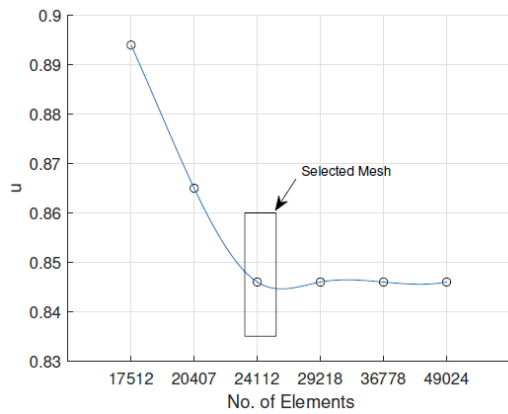


Figure 3 Dimensionless axial velocity component at $x = 2$ in the channel. ($Re=150, \phi = 0.04, Mn_f=70$)

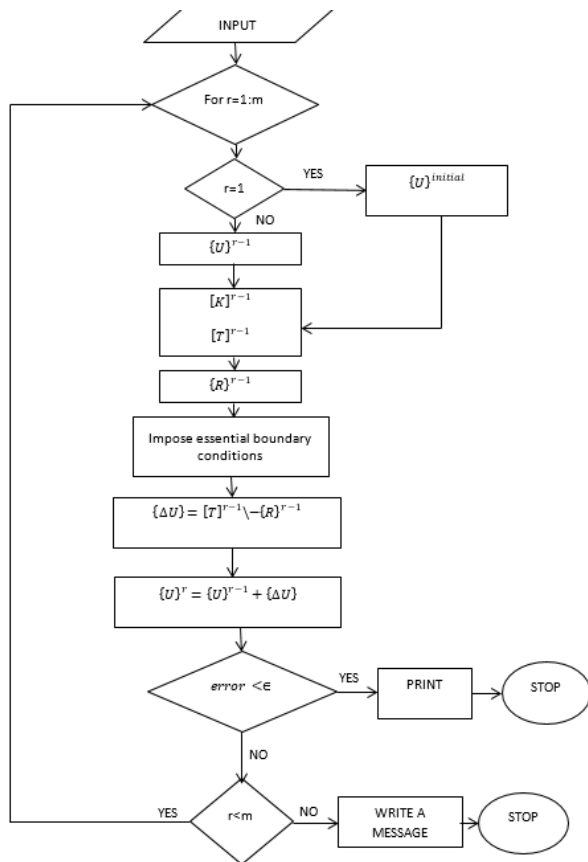


Figure 4 Flowchart of Newton-Raphson nonlinear scheme

2.6 Validations

The present formulation is validated against several data available in literature. The first comparison is made against benchmark case of pure fluid with $Pr = 0.71$ in the enclosure. The average Nusselt number subjected to various Rayleigh number are well agreed with [27, 30] as shown in Table 1. Second validation involves water-copper nanofluid simulated in a cavity. The temperature under the influence of Grahshof numbers agrees well with [27] as depicted in Figure 5. In the last case, the formulation is validated against

MHD natural convection in an enclosure filled with water- Al_2O_3 nanofluid. Nusselt number is studied in term of nano-fractions and Rayleigh numbers. As shown in Table 2 these numerical results are in good agreement with those obtained in [18].

Table 1 Comparison of present average nusselt result with other literature works for different Rayleigh number at $Pr = 0.71$.

Ra	Present	Khanafar [27]	De Vahl Davis [30]
10^3	1.118	1.118	1.118
10^4	2.243	2.245	2.243
10^5	4.518	4.522	4.519

Table 2 Average Nusselt number under various Rayleigh number and nano fraction at $Ha = 30$

	$\phi = 0$	$\phi = 0.02$	$\phi = 0.04$	$\phi = 0.06$
Ra Present $=10^3$	1.002	1.063	1.126	1.191
[18]	1.002	1.060	1.121	1.184
Ra Present $=10^4$	1.177	1.195	1.227	1.270
[18]	1.183	1.212	1.249	1.291
Ra Present $=10^5$	3.092	3.021	2.958	2.902
[18]	3.150	3.138	3.124	3.108

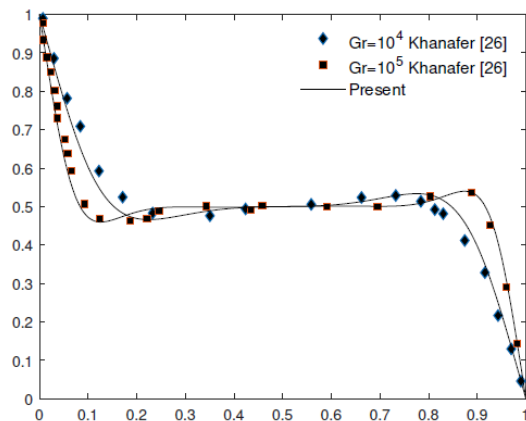


Figure 5 Comparison of the temperature at the mid cavity between [27] and present results ($Pr=6.2, \phi = 0.1, Gr=104, 105$)

3.0 RESULTS AND DISCUSSION

Electro-conducting and nonconducting nanofluids are studied under the exposure of spatial varying magnetic field. Fe_3O_4 nanoparticle of crude-oil based nanofluid is investigated in a channel flow. The thermophysical properties of crude oil based fluid and nanoparticles are shown in Table 3. Computations are made for a range of Hartmann numbers ($Ha = 0$ to 1), magnetic numbers ($Mn_f = 0$ to 300) and nano volume fraction ($\phi = 0$ to 0.1). The walls are $10m$ in length and

separated by a distance $h = 0.02$ m. The temperature of the walls is $\bar{T}_w = 50$ °C whereas $\bar{T}_f = 35$ °C. The nanoparticle has reached its saturation at the magnetization, $M_r = 60$ A/m. Other governing parameters such as temperature number ε , Prandtl Pr and Eckert number Ec are fixed at 7×10^{-8} , 63.5 and 1.23×10^{-7} , respectively.

Table 3 Thermophysical properties of crude oil and Fe₃O₄

	ρ kg/m ³	c_p J/kgK	k W/mK	$\beta \times 10^{-5}$ K ⁻¹	σ S/m
Crude oil [31, 32]	822	2008	0.158	70	208.8×10^{-9}
Iron Oxide (Fe ₃ O ₄) [18]	5200	670	6	1.3	25000

3.1 Nusselt Number

Figure 6 illustrates the effect of magnetic number, Mnf, Hartman number, Ha at the constant Reynold number Re and Fe₃O₄ nano-fraction on the local and average Nusselt numbers.

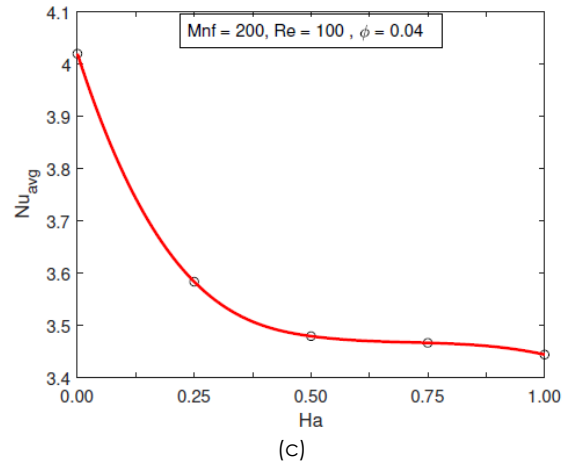
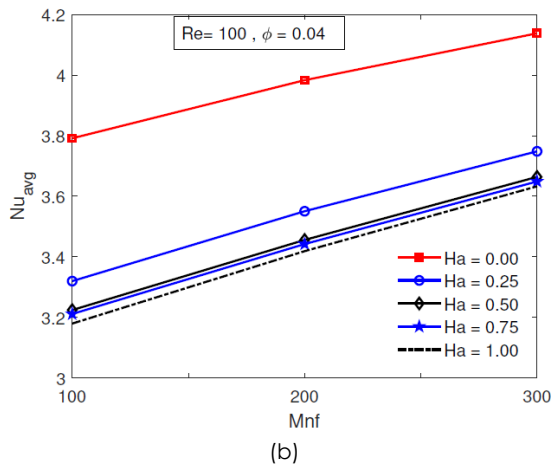
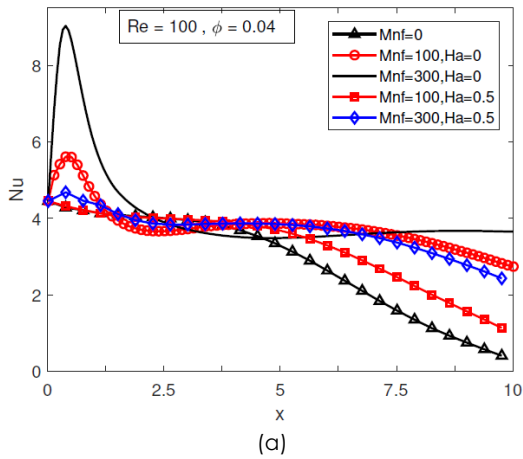
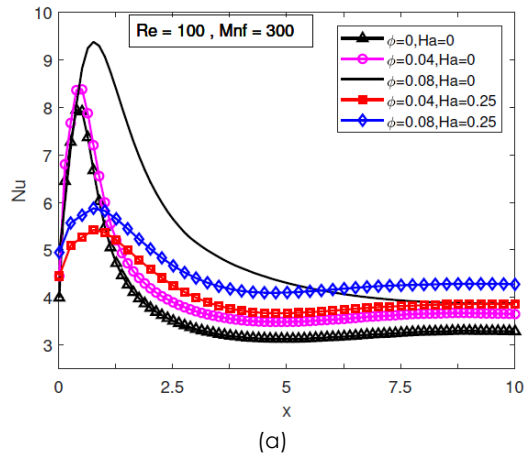


Figure 6 Variation of Hartmann number, magnetic number for Nusselt number along the lower wall

Figure 6(a) shows the local Nusselt number increases with the magnetic number. The fluid region in the proximity of the magnetic source experiences the greatest increment in the temperature. In contrast, it is observed that Nusselt number decreases with the increase in Hartman number. This also indicates that, for the conducting crude oil nanofluid, the convection flow is suppressed under the exposure of Lorentz force represented by Hartmann number. Nevertheless, in all cases, the disturbance due to the magnetic field on temperature has been felt far downstream.

The average Nusselt number of crude oil-nanofluid against varying magnetic number and for various Hartmann numbers is shown in Figure 6(b). It is demonstrated that the Nusselt number increases almost linearly with the magnetic number but reduces with the increasing Hartmann number. For Hartmann number greater than 0.5, the heat enhancement remains almost constant as shown in Figure 6(c). It is being observed that conduction dominates the flow and a further increase in Hartmann number will not affect the heat transfer mechanism.



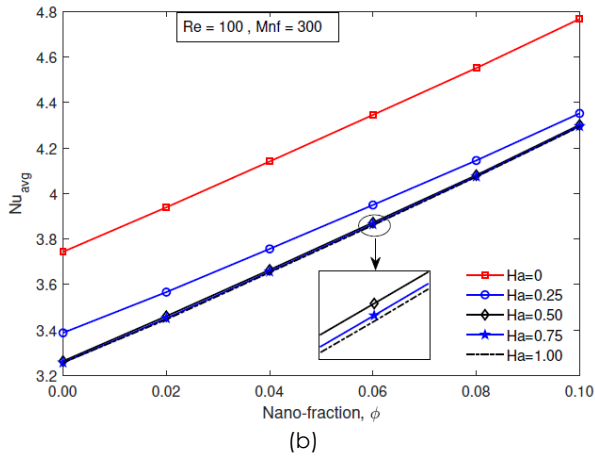


Figure 7 Variation of Hartmann number, nano-fraction for Nusselt number along the lower plate

Figure 7 shows the effect of Fe₃O₄ nano-fraction and Hartmann number at the constant Reynold and magnetic numbers on the local and average Nusselt numbers.

Figure 7(a) shows the increment of local Nusselt number with the addition of nano fraction. This indicates the susceptibility of magnetisation posed by metal nanoparticle is effective in controlling heating at the targeted region. In contrast, it is also observed that Nusselt number decreases with the increase in Hartman number. Similar trend has also been reported in [21].

Figure 7(b) shows how the addition of nanoparticles influences the average Nusselt number. It is obvious that regardless of the variation of Hartmann number, the Nusselt number has increased linearly with nano-fraction. As the Hartmann number increases, the Nusselt number along the wall decreases. This is caused by the domination of conduction mechanism over the convection flow. The enhancement occurs mainly because of the high thermal conductivity properties of the nanoparticle.

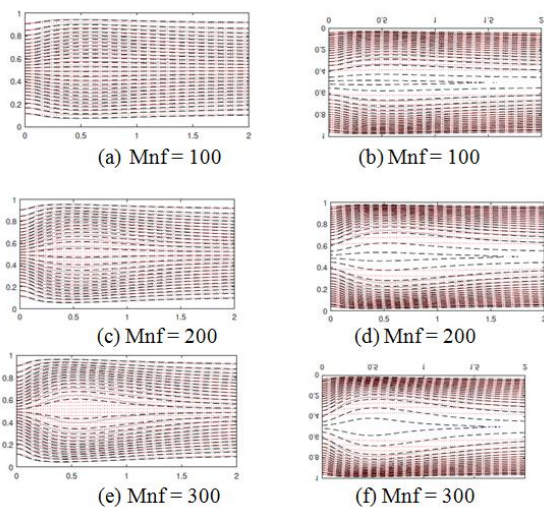
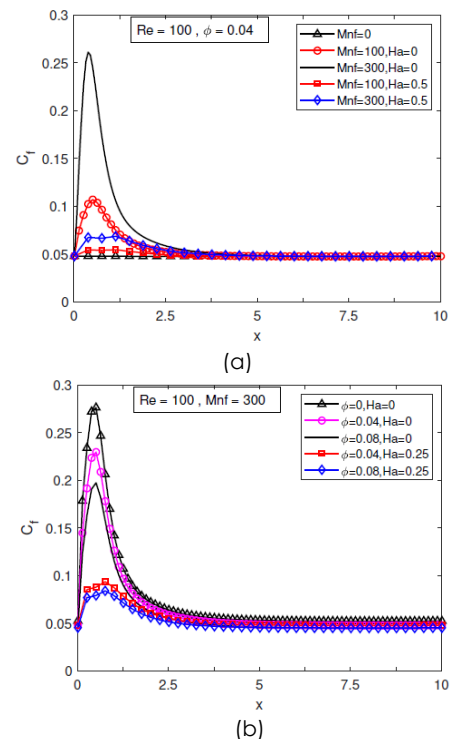


Figure 8 Comparison of streamlines (left column) and isotherms (right column) for Re = 150. Oil (—), nanofluids $\phi = 0.04$ (- -) and nanofluids with Ha=0.25 (...)

Figure 8 illustrates a comparison between crude oil ($\phi = 0$) and Fe₃O₄-nanofluid ($\phi = 0.04$) in terms of streamlines and isotherms for 2 unit length of channel. The results are presented for three values of magnetic number (Mnf = 100, 200, 300) and a single value of Hartmann number (Ha = 0.25). By increasing the magnetic number, the heated nanofluid tends to move towards the wall. The stream function increases with the magnetic number indicating the strength of convective flow increases. This fluid movement become obvious at sufficiently high magnetic strength. As the nano fraction increases, the intensity of streamlines also increases due to the energy transport through the flow. However, adverse observation is made when Lorentz force is introduced into the flow field. The conduction mechanism becomes dominant whereby the isothermal and stream lines are parallel to each other. This outcome agrees with the finding of [18, 20]. It also observed that the flow pattern of nanofluid is affected significantly by magnetic number and Hartmann number.

3.2 Skin Friction

Figure 9 shows the effect of magnetic number, MnF, Hartmann number, Ha, nano fraction and Reynold number, Re on the local and average skin friction coefficient along the lower plate. Figure 8(a) indicates the variation of the local skin friction coefficient at constant Reynolds number. It is observed that the skin coefficient increases with the increase in magnetic number. However, the presence of Hartman number has lowered the skin friction. Such trend varies similarly with the local Nusselt number at the magnetic strength concerned.



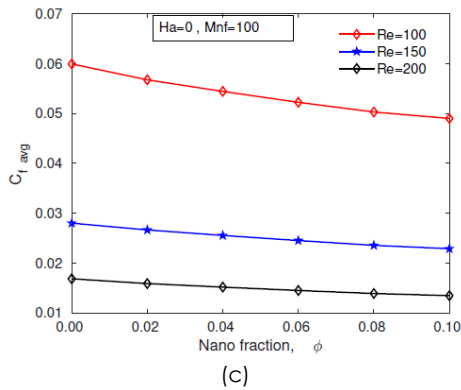


Figure 9 Variation of Hartmann number, magnetic number and Reynolds number for skin friction coefficient

Figure 9(b) presents the variation of nano fraction and Hartmann number at the magnetic number $Mnf = 300$. At constant Hartmann number, the local skin friction coefficient decreases with increasing nano fraction and Hartmann number. Both Figure 9(a) and Figure 9(b) indicate that the significant variation of skin coefficient happens at the proximity of magnetic source for both magnetic and Hartmann numbers. Beyond the region, $x \approx 1.5$, the skin friction decreases accordingly and regains its initial value corresponding to fully developed flow. The positive values indicate that there is no inversion of crude oil nanofluid flow.

Figure 9(c) depicts the average skin friction for the variation of Reynolds numbers ($Re = 100, 150, 300$) and nano fractions in the range of $0 \leq \phi \leq 0.1$. It is noticed that the skin friction has an inverse relationship with the increasing nano fractions and Reynolds numbers.

3.3 Magnetic Field Heating for EOR

The numerical model is used to study the heat transfer of a variation of nanoparticle such as Fe_3O_4 , Al_2O_3 , CuO , Cu in crude oil whose properties are given in Table 4. As such, the variation of Nusselt for different nanoparticles, nano-fraction and magnetic number are compared at $Re = 100$ as shown in Figure 10.

Table 4 Thermophysical properties of crude oil and nanoparticle

	ρ kg/m ³	c_p J/kgK	k W/mK	$\beta \times 10^{-5}$ K-1	σ S/m
Crude oil [31, 32]	822	2008	0.158	70	208.8×10^{-9}
Iron Oxide (Fe_3O_4) [18]	5200	670	6	1.3	25000
Aluminium oxide (Al_2O_3) [33]	3970	765	25	0.85	10^{-12}
Copper(II) oxide (CuO) [33]	6500	540	18	0.85	10^{-10}
Copper (Cu) [33]	8933	385	401	1.67	5.96×10^7

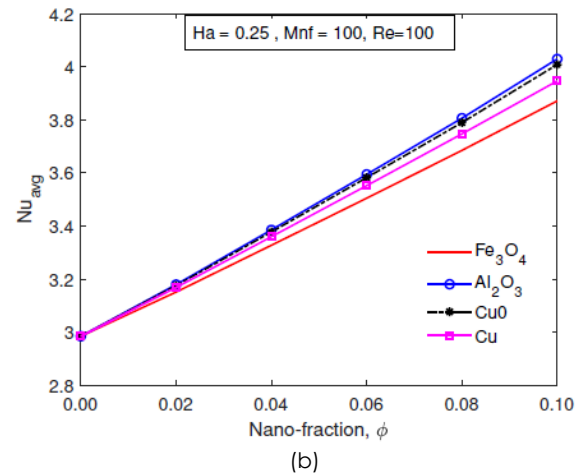
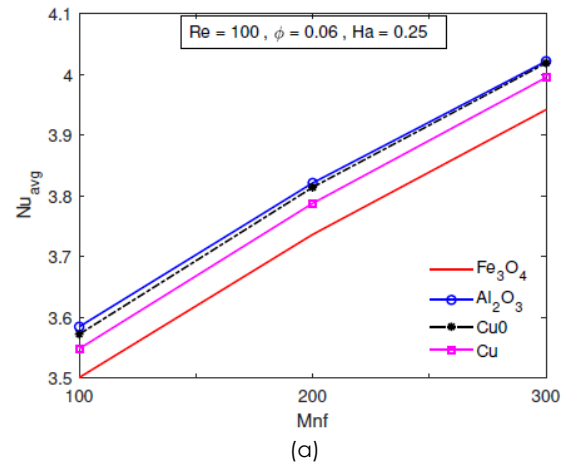


Figure 10 Variation of magnetic number and nano-fraction for Nusselt number at lower wall for different nanoparticles

Figure 10(a) shows that the heat transfer of all crude oil based nanoparticle increases linearly with the magnetic number for $\phi = 0.06$ nano fraction and 0.25 Hartmann number. Among the crude oil nanofluid, the Al_2O_3 nanofluid has the highest rate of heat transfer while Cu has the lowest rate of heat transfer.

Figure 10(b) shows the comparison between nano-fraction for Fe_3O_4 , Al_2O_3 , CuO , Cu nanoparticles under constant magnetic strength and Reynolds number. All nanoparticles exhibit similar heat enhancement behaviour which is a linear increment with subsequent increment in nano fraction. Al_2O_3 is shown as having the highest enhancement of heat transfer as compared to other nanoparticles. This may be due to the low electrical conductivity possessed by the Al_2O_3 nanoparticle. Both Al_2O_3 and CuO nanoparticle have the lowest electrical conductivity but the slightly higher thermal conductivity of the former make it a better agent of heating. On the other hand, although Cu has the highest thermal conductivity, it is accompanied by high electrical conductivity which reduces the efficiency of the heat transfer.

The result indicates that the effect of thermal conductivity and electrical conductivity of nanofluid

are significant in determining the heat transfer under the influence of the magnetic field. The results suggest that heat transfer enhancement can be made by utilising the nanoparticle with low electrical conductivity and higher thermal conductivity as it can maximise the thermal heating of crude oil in EOR.

4.0 CONCLUSION

A numerical model based on FEM has been developed in predicting the crude oil-nanofluid flow and heat transfer in reservoir formation. The influence of applied magnetic field based on the FHD and MHD principles have been theoretically studied. In the investigation, the addition of nanoparticle has been shown to be able to increase the rate of heat transfer of the fluid system. It is established that the performance of heat transfer is highly dependent on the Hartmann number and magnetic number. The applied magnetic field has increased the thermal energy in the presence of the nanoparticle. This indicates that high thermal conductivity of nanoparticle is dominant in generating a higher thermal rate of recovery. However, a reverse effect has been observed with the presence of Lorentz force represented by Hartmann number. Results of the study thus suggested that nanoparticle with low electrical conductivity and high thermal conductivity is effective in providing thermal energy to the EOR. In conclusion, this study highlights the potential of mixing nanoparticles into crude oil in enhancing heat transfer mechanism for EOR.

Acknowledgement

This work is supported by the Fundamental Research Grant Scheme (FRGS No. 0153AB-K57) funded by Ministry of Higher Education of Malaysia.

References

- [1] M. Blunt, F. J. Fayers, and F. M. Orr Jr. 1993. Carbon Dioxide in Enhanced Oil Recovery. *Energy Conversion and Management*. 34(9-11): 1197-1204. [https://doi.org/10.1016/0196-8904\(93\)90069-M](https://doi.org/10.1016/0196-8904(93)90069-M).
- [2] S. Thomas. 2008. Enhanced Oil Recovery-An Overview. *Oil & Gas Science and Technology-Revue de l'IFP*. 63(1): 9-19. <https://doi.org/10.2516/ogst:2007060>.
- [3] I. D. Gates and S. R. Larter. 2014. Energy Efficiency and Emissions Intensity of Sagd. *Fuel*. 115: 706-713. <https://doi.org/10.1016/j.fuel.2013.07.073>.
- [4] G. Giacchetta, M. Leporini, and B. Marchetti. 2015. Economic and Environmental Analysis of a Steam Assisted Gravity Drainage (Sagd) Facility for Oil Recovery from Canadian Oil Sands. *Applied Energy*. 142: 1-9. <https://doi.org/10.1016/j.apenergy.2014.12.057>.
- [5] K. Jha and A. Chakma. 1999. Heavy-oil Recovery from Thin Pay Zones by Electromagnetic Heating. *Energy Sources*. 21(1-2): 63-73. <https://doi.org/10.1080/00908319950014966>.
- [6] A. Chhetri and M. Islam. 2008. A Critical Review of Electromagnetic Heating for Enhanced Oil Recovery. *Petroleum Science and Technology*. 26(14): 1619-1631. <https://doi.org/10.1080/10916460701287607>.
- [7] R. W. Fox, A. T. McDonald, and P. J. Pritchard. 1985. *Introduction to Fluid Dynamics*. John Wiley and Sons, New York. 354.
- [8] A. Bera and T. Babadagli. 2015. Status of Electromagnetic Heating for Enhanced Heavy Oil/Bitumen Recovery and Future Prospects: A Review. *Applied Energy*. 151: 206-226. <https://doi.org/10.1016/j.apenergy.2015.04.031>.
- [9] A. Sadeghi, H. Hassanzadeh, and T. G. Harding. 2017. A Comparative Study of Oil Sands Preheating Using Electromagnetic Waves, Electrical Heaters and Steam Circulation. *International Journal of Heat and Mass Transfer*. 111: 908-916. <https://doi.org/10.1016/j.ijheatmasstransfer.2017.04.060>
- [10] Y. H. Shokrlu and T. Babadagli. 2014. Viscosity Reduction of Heavy Oil/Bitumen Using Micro-and Nano-metal Particles during Aqueous and Non-aqueous Thermal Applications. *Journal of Petroleum Science and Engineering*. 119: 210-220. <https://doi.org/10.1016/j.petrol.2014.05.012>.
- [11] M. M. Abdulrahman and M. Meribout. 2014. Antenna Array Design for Enhanced Oil Recovery under Oil Reservoir Constraints with Experimental Validation. *Energy*. 66: 868-880. <https://doi.org/10.1016/j.energy.2014.01.002>.
- [12] J. Greff and T. Babadagli. 2013. Use of Nano-metal Particles as Catalyst under Electromagnetic Heating for In-situ Heavy Oil Recovery. *Journal of Petroleum Science and Engineering*. 112: 258-265. <https://doi.org/10.1016/j.petrol.2013.11.012>.
- [13] R. Santoso, S. Rachmat, A. Resha, W. Putra, H. Hartowo, O. Setiawati et al. 2016. An Investigation of Fe₂O₃ Nanoparticles Diffusion into Oil for Heat Transfer Optimisation on Electromagnetic Heating for Well Stimulation and eor. *SPE Asia Pacific Oil & Gas Conference and Exhibition*. 1em plus 0.5em minus 0.4em Society of Petroleum Engineers, <https://doi.org/10.2118/182152-MS>.
- [14] A. Davidson, C. Huh, S. L. Bryant et al. 2012. Focused Magnetic Heating Utilizing Superparamagnetic Nanoparticles for Improved Oil Production Applications. *SPE International Oilfield Nanotechnology Conference and Exhibition*. 1em plus 0.5em minus 0.4em Society of Petroleum Engineers. <https://doi.org/10.2118/157046-MS>.
- [15] M. Liu, G. Zhao et al. 2013. A Performance Comparison Study of Electromagnetic Heating and Sagd Process. *SPE Heavy Oil Conference-Canada*. 1em plus 0.5em minus 0.4em Society of Petroleum Engineers. <https://doi.org/10.2118/165547-MS>.
- [16] A. Davletbaev, L. Kovaleva, and T. Babadagli. 2014. Heavy Oil Production by Electromagnetic Heating in Hydraulically Fractured Wells. *Energy & Fuels*. 28(9): 5737-5744. <https://doi.org/10.1021/ef5014264>.
- [17] M. Bientinesi, L. Petarca, A. Cerutti, M. Bandinelli, M. De Simoni, M. Manotti, and G. Maddinelli. 2013. A Radiofrequency/Microwave Heating Method for Thermal Heavy Oil Recovery Based on a Novel Tight-shell Conceptual Design. *Journal of Petroleum Science and Engineering*. 107: 18-30. <https://doi.org/10.1016/j.petrol.2013.02.014>.
- [18] B. Ghasemi, S. Aminossadati, and A. Raisi. 2011. Magnetic Field Effect on Natural Convection in a Nanofluid-filled Square Enclosure. *International Journal of Thermal Sciences*. 50(9): 1748-1756. <https://doi.org/10.1016/j.ijthermalsci.2011.04.010>.
- [19] M. Mansour and M. Bakier. 2015. Influence of Thermal Boundary Conditions on Mhd Natural Convection in Square Enclosure Using Cu-Water Nanofluid. *Energy Reports*. 1: 134-144. <https://doi.org/10.1016/j.egyr.2015.03.005>.
- [20] M. Sheikholeslami and D. D. Ganji. 2014. Ferrohydrodynamic and Magnetohydrodynamic Effects on Ferrofluid Flow and Convective Heat Transfer. *Energy*. 75: 400-410. <https://doi.org/10.1016/j.energy.2014.07.089>.
- [21] N. S. Gibanov, M. A. Sheremet, H. F. Oztop, and O. K. Nusier. 2017. Convective Heat Transfer of Ferrofluid in a Lid-driven Cavity with a Heat-conducting Solid Backward Step under

- the Effect of a Variable Magnetic Field. *Numerical Heat Transfer, Part A: Applications*. 72(1): 54-67. <https://doi.org/10.1080/10407782.2017.1353377>.
- [22] M. Sheikholeslami, M. Gorji-Bandpy, and D. Ganji. 2014. Investigation of Nanofluid Flow and Heat Transfer in Presence of Magnetic Field Using Kkl Model. *Arabian Journal for Science and Engineering*. 39(6): 5007-5016. <https://doi.org/10.1007/s13369-014-1060-4>.
- [23] R. E. Rosensweig. 2013. *Ferrohydrodynamics*. Courier Corporation.
- [24] G. D. Smith. 1985. *Numerical Solution of Partial Differential Equations: Finite Difference Methods*. Oxford University Press.
- [25] H. K. Versteeg and W. Malalasekera. 2007. *An Introduction to Computational Fluid Dynamics: The Finite Volume Method*. Pearson Education.
- [26] H. Matsuki, K. Yamasawa, and K. Murakami. 1977. Experimental Considerations on a New Automatic Cooling Device Using Temperature-Sensitive Magnetic Fluid. *IEEE Transactions on Magnetics*. 13(5): 1143-1145. <https://doi.org/10.1109/TMAG.1977.1059679>.
- [27] K. Khanafer, K. Vafai, and M. Lightstone. 2003. Buoyancy-driven Heat Transfer Enhancement in a Two-dimensional Enclosure Utilizing Nanofluids. *International Journal of Heat and Mass Transfer*. 46(19): 3639-3653. [https://doi.org/10.1016/S0017-9310\(03\)00156-X](https://doi.org/10.1016/S0017-9310(03)00156-X).
- [28] H. Brinkman. 1952. The Viscosity of Concentrated Suspensions and Solutions. *The Journal of Chemical Physics*. 20(4): 571-571. <https://doi.org/10.1063/1.1700493>.
- [29] J. C. Maxwell. 1881. *A Treatise on Electricity and Magnetism*. Clarendon Press. 1.
- [30] G. de Vahl Davis. 1983. Natural Convection of Air in a Square Cavity: A Bench Mark Numerical Solution. *International Journal for Numerical Methods in Fluids*. 3(3): 249-264. <https://doi.org/10.1002/flid.1650030305>.
- [31] W. Rukthong, P. Piumsomboon, W. Weerapakkaron, and B. Chalermisinsuwan. 2016. Computational Fluid Dynamics Simulation of a Crude Oil Transport Pipeline: Effect of Crude Oil Properties. *Engineering Journal (Eng. J.)*. 20(3): 145-154. <https://doi.org/10.4186/ej.2016.20.3.145>.
- [32] M. Mohammadi and F. Mohammadi. 2016. Parametric Study on Electrical Conductivity of Crude Oils; Basis Experimental Data. *Petroleum & Coal*. 58(6).
- [33] M. Sheikholeslami, S. Abelman, and D. D. Ganji. 2014. Numerical Simulation of Mhd Nanofluid Flow and Heat Transfer Considering Viscous Dissipation. *International Journal of Heat and Mass Transfer*. 79: 212-222. <https://doi.org/10.1016/j.ijheatmasstransfer.2014.08.004>.